EFFECT OF PROCESSING ROUTE ON STRAIN CONTROLLED LOW CYCLE FATIGUE BEHAVIOR OF POLYCRYSTALLINE NiAL

K. Bhanu Sankara Rao, B.A. Lerch and R.D. Noebe

NASA Lewis Research Center
21000 Brookpark Road
Cleveland, Ohio 44135

Abstract

The present investigation examines the effects of manufacturing process on the total axial strain controlled low cycle fatigue behavior of polycrystalline NiAl at 1000 K, a temperature above the monotonic brittle-to-ductile transition temperature (BDTT). The nickel aluminide samples were produced by three different processing routes: hot isostatic pressing of prealloyed powders, extrusion of prealloyed powders, and extrusion of vacuum induction melted ingots. The LCF behavior of the cast plus extruded material was also determined at room temperature (below the BDTT) for comparison to the high temperature data. The cyclic stress response, cyclic stress-strain behavior, and strain-life relationships were influenced by the alloy preparation technique and the testing temperature. Detailed characterization of the LCF tested samples was conducted by optical and electron microscopy to determine the variations in fracture and deformation modes and to determine any microstructural changes that occurred during LCF testing. The dependence of LCF properties on processing route was rationalized on the basis of starting microstructure, brittle-to-ductile transition temperature, deformation induced changes in the basic microstructure, deformation substructure, and synergistic interaction between the damage modes.

Fatigue and Fracture of Ordered Intermetallic Materials: II
Edited by W.O. Soboyejo, T.S. Srivatsan and R.O. Ritchie
The Minerals, Metals & Materials Society, 1995

Introduction

There would be considerable benefit in developing new structural materials where high use temperatures and strength coupled with low density are minimum capabilities. In pursuing this goal, ordered intermetallic alloys have been the subject of intensive investigation for at least the last decade. Of the many intermetallic alloys under initial consideration, NiAl is one of the few systems that has emerged as a promising candidate for further development. This is due to a number of property advantages including low density, high melting temperature, high thermal conductivity, excellent environmental resistance, a relatively low brittle-to-ductile transition temperature (BDTT), and the potential for significantly improving creep resistance through alloying[1-4].

However, B2 nickel aluminides are challenged by a lack of ambient temperature ductility and toughness. These deficiencies severely limit possible applications and impose limits on the fabrication and forming of these materials. The lack of ductility at room temperature has been attributed to an inherently low cleavage stress, which is partly attributed to a low mobile dislocation density, and the inability to initiate a sufficient number of independent slip systems to satisfy the von Mises criterion for generalized plasticity of a polycrystalline aggregate [2-7]. Efforts at resolving these problems in NiAl have met with little success. Ductility improvements through ternary alloying additions have been unsuccessful to date except in the case of Fe, Ga, or Mo additions to single crystal NiAl; where improvements in ductility from 1% to nearly 6% were achieved [1,8]. However, due to the grain boundary compatibility issue, no similar improvements in ductility have been reported in polycrystalline alloys [7, 9-11]. However, improvements in the processing and compositional control of binary stoichiometric NiAl have resulted in limited, but at least consistent and reproducible, room temperature ductilities on the order of 1-3% [4,7,10,12-15]. These polycrystalline alloys are typically produced by extrusion of cast ingots.

At intermediate temperatures and moderate strain rates, tensile ductility is no longer a serious limitation. Extruded NiAl undergoes a dramatic brittle-to-ductile transition in the range of 550 - 700 K. Significant increases in tensile elongation [3,7,10,12,14], fracture strength [7,10,12,14] and fracture toughness [16-18] have been reported in this temperature range with an associated tendency towards more ductile fracture [6,7,14]. Several studies have suggested that thermally activated deformation processes, such as localized dislocation climb, provide the additional deformation mechanisms necessary to maintain grain boundary compatibility, thus, contributing to the sharp transition from brittle to ductile behavior [5,7,14,19].

While a reasonable understanding of the monotonic flow and fracture behavior of polycrystalline NiAl has been achieved [1-19], much less is known about the cyclic behavior of NiAl alloys. Consequently, specific attention has recently been directed toward the strain controlled low cycle fatigue (LCF) behavior of polycrystalline NiAl at room and elevated temperatures [20-24]. Lerch and Noebe [20,24] have performed room temperature and 1000 K fatigue tests on cast plus extruded polycrystalline NiAl at plastic strain ranges between 0.06% and 0.2% at a total strain rate of 10^{-3} s^{-1}. At room temperature NiAl work hardened continuously during testing and failed in a predominantly intergranular mode [20]. Similar room temperature behavior has been observed by Edwards and Gibala [21]. At 1000 K, very little change in the stress response occurs over the life of the test and the fatigue life behavior follows the typical Coffin-Manson relationship [24].

Cullers et al. [22,23] evaluated the LCF deformation of powder extruded NiAl between 600 K and 700 K employing rather high plastic strain ranges of 0.5% and 1.0%. These tests were performed very near the BDTT of the material and fatigue lives were limited to 1000 - 3000 cycles. In this temperature range, the cyclic stress response displayed three stages of behavior; the material work hardened for the first few cycles and then reached a plateau, followed by an additional region of work hardening very near the end of sample life. As the test temperature was increased or strain range decreased, both the initial hardening rate and relative saturation stress decreased. These changes in stress response have been correlated with the continuously evolving dislocation structures during the LCF tests.

Though many of the LCF studies were conducted on cast and extruded material [20,21,24], in actual applications the components may likely be manufactured to near net shape, by powder metallurgy techniques such as hot isostatic pressing (HIP), forging, or powder extrusion (PE). Powder metallurgy processing techniques have the advantage of being both economical and reproducible. These benefits are due in part to the ability to obtain near net shape components that significantly limits the amount of post-process machining. However, the soundness of the product depends on the purity of the starting powders and the amount of residual porosity at the end of processing. In addition, the naturally occurring oxide scales on the powder particles result in prior particle boundaries after consolidation. While prior particle boundaries are generally broken up during extrusion can be a serious concern in hipped consolidated components. Non-metallic inclusions and porosity have been shown to decrease the LCF life of powder metallurgy nickel-based superalloys [25]. These imperfections have been shown to act as sites for crack initiation, with their detrimental effects more pronounced in relatively hard materials of limited flow capacity [26]. Furthermore, hip consolidation of powders requires relatively long exposure times at high temperatures that generally results in a product with larger grains. Coarse grain size is detrimental in that it accentuates the synergistic interactions between LCF damage, creep and oxidation at elevated temperatures [27,28]. The effect of creep and oxidation on an alloy's cyclic life can be considerable, reducing it by orders of magnitude [29,30].

Consequently, with limited data available for intermetallics there is a need to asses the effects of processing route on cyclic properties of nickel aluminides. Therefore, the present investigation was undertaken to characterize the effects of processing on the LCF life and cyclic stress response of polycrystalline NiAl at 1000 K. The processing routes employed include the more common extrusion of cast ingots (CE), extrusion of prealloyed powders (PE), and hot isostatic pressing (HIP) of prealloyed powders. For comparison, data on the CE material tested at 300 K is also presented. A detailed examination of the microstructural changes and the crack initiation and propagation behavior has also been conducted with a view to understanding the features that may influence the LCF life and cyclic stress response at room and elevated temperatures.

Experimental procedures

Material processing

Hipped Processed NiAl (HP): Vacuum atomized -20/+325 mesh prealloyed powders of stoichiometric NiAl were obtained from Homogeneous Metals, Inc (Heat P1418). The powder was packed into two 304 stainless steel cans approximately 96 mm in diameter by 150 mm in length. The cans were evacuated and hot isostatically pressed at 1533 K and at a pressure of 241 MPa for 5 hours. These hipping conditions are essentially the minimum

necessary to produce full consolidation while minimizing time at temperature.
Powder Extruded NiAl (PE): A second heat of vacuum atomized powder was also obtained from Homogeneous Metals, Inc (Heat P2098). From this heat, -100/+325 mesh powder was packed into mild steel extrusion cans that were subsequently evacuated and extruded at 1200 K at an area reduction ratio of 12:1.
Cast & Extruded NiAl (CE): Cast and extruded NiAl material was produced by vacuum induction melting commercially pure Ni and Al at the equiatomic composition and casting into copper chill molds. Two cropped NiAl ingots, nominally 38 mm in diameter and 95 mm in length, were canned in mild steel and extruded at 1200 K at an area reduction ratio of 12:1.

Low cycle fatigue testing

Cylindrical fatigue samples, 13 mm in diameter by 127 mm in length (Fig. 1) were ground from either the extruded bars or electro-discharge machined blanks of NiAl. To facilitate

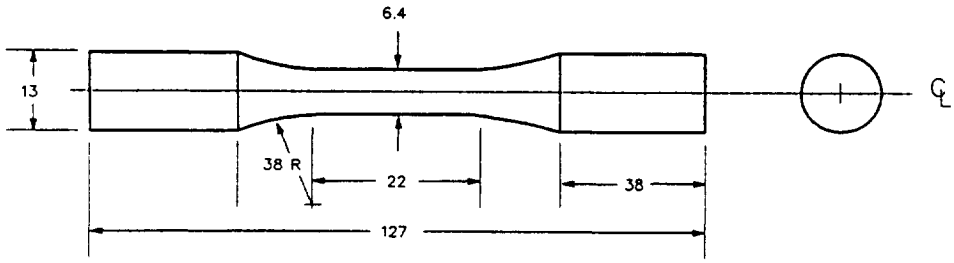

Figure 1 - Geometry of low cycle fatigue specimen (All dimensions are in mm).

the observation of deformation and damage, the reduced gage section of each specimen was electropolished in a 10% perchloric acid-90% methanol solution at 20-25 volts, 1 amp, and 208 K prior to LCF testing. LCF tests were performed at 300 and 1000 K in air under a fully-reversed, axial strain-controlled mode. A triangular strain-time waveform was employed for the tests conducted over strain amplitudes in the range 0.1 to 0.5% and at a strain rate of $10^{-3}s^{-1}$.

Since room temperature notch sensitivity and brittleness of this material precluded the welding of thermocouples onto the test specimens, temperature was measured and controlled by an infrared pyrometer. The temperature gradient along the gage length was determined with a NiAl control specimen that had three thermocouples spot welded along the gage length. The temperature gradient was no more than ± 5 K at the 1000 K test temperature. The infrared pyrometer was also calibrated to this thermocoupled control specimen.

Microstructural characterization

The fracture surfaces of fatigued samples were examined by scanning electron microscopy (SEM) paying special attention to the mechanisms of crack initiation and propagation. The deformation substructure was evaluated by transmission electron microscopy (TEM). Samples for TEM examination were taken from thin slices cut from gage portions of the fatigue specimens. The slices were mechanically thinned to 150μm followed by electrolytic

thinning to 1000 Å in a bath containing 70 pct. ethanol, 14 pct. distilled water, 10 pct. butylcellusolve, and 6 pct. perchloric acid at a potential of 25V and at temperatures between 263-268 K. Thin foils were examined in a JEOL 100C microscope operating at an accelerating voltage of 120 keV.

RESULTS

Chemical composition and microstructure

The average chemical composition and grain size of NiAl obtained at the end of different processing routes are given in Table I. Grain size distribution was measured as recommended in ASTM standards E112 and E1181. The HP alloy had larger grains and a

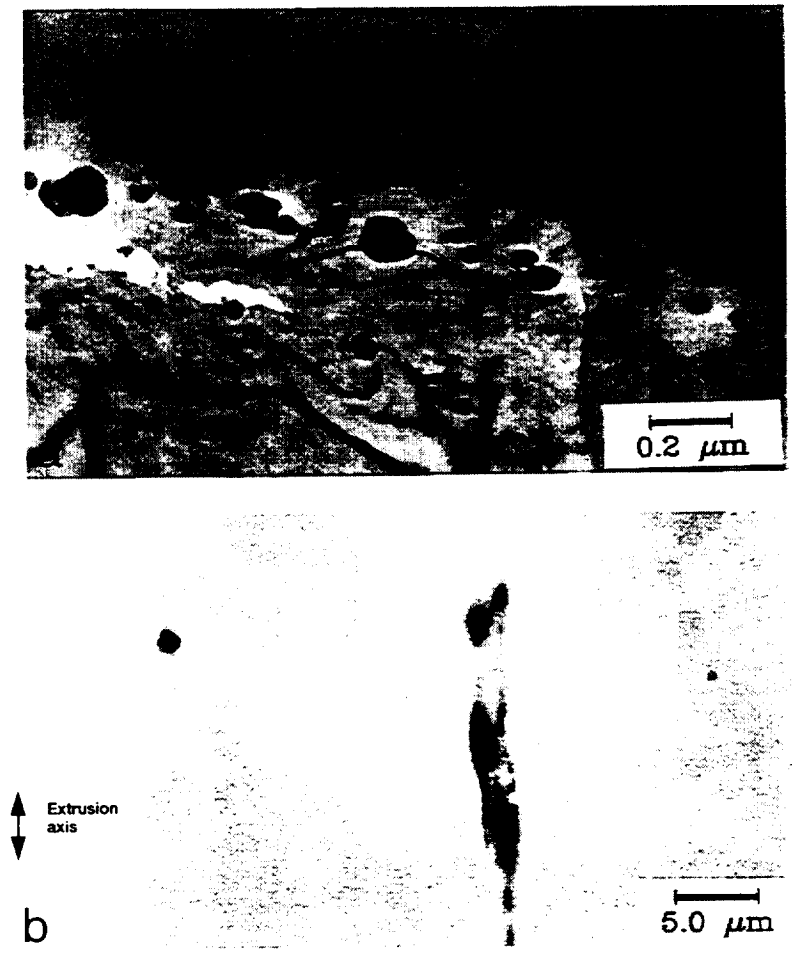

Figure 2 - a) TEM micrograph showing alumina particles in HP NiAl; b) SEM micrograph of CE material indicating casting void that remained after the extrusion process.

Table I - Composition and Grain Size of NiAl

Fabrication Method	Grain Size, μm	Composition, at%					
		Ni	Al	O	C	S	N
HP-hipped powder (Heat P1418)	70±14	50.5*	49.5*	0.028	0.014	<0.002	<0.0006
PE-extruded powder (Heat P2098)	12±3	50.2*	49.7*	0.025	0.017	<0.0017	0.0009
CE cast + extruded	18±3	50**	50**	0.011	0.029	<0.002	<0.003

* Determined by wet chemical analysis methods, ±0.2 at % within a 95% confidence interval

** Nominal composition

larger variation in grain size compared to the fully recrystallized extruded materials (CE and PE). The HP material contained prior particle boundaries that were composed of narrow stringers of fine Al_2O_3 particles (Fig. 2a). The CE material contained internal voids, which were aligned parallel to the extrusion axis (Fig. 2b). Despite the 12:1 reduction ratio during extrusion, this material contained residual porosity, probably owing to the presence of entrapped gas. The PE alloy was fully consolidated with fewer defects than the CE or HP material.

Monotonic behavior

The monotonic tensile behavior for the materials investigated is shown in Table II. At room temperature, the HP material had zero tensile ductility and therefore, was not fatigue tested at this temperature. The two extruded materials did exhibit limited tensile ductility, on the order of 1%. With increasing temperature NiAl reaches a very sudden brittle-to-ductile transition, occurring over a very narrow temperature range. However, the specific transition temperature is dependent on strain rate, composition, grain size and processing condition [3,6,7,14,18,24]. Therefore, the BDTT's for the materials investigated in this study are listed in Table II for a strain rate of 10^{-3} s^{-1}. As evident from Table II, a test temperature of 1000 K represents a condition above the BDTT for all the materials investigated, regardless of processing route. Above the BDTT, all three materials exhibit extensive tensile ductility ($\geq$25%) before fracture and a fracture toughness greater than 30 MPa$\sqrt{m}$ [16-18]. The initial yield portion of the monotonic tensile stress-strain curves at 1000 K is shown in Fig. 3. The elastic moduli determined from the 1000 K tensile tests were 160, 125

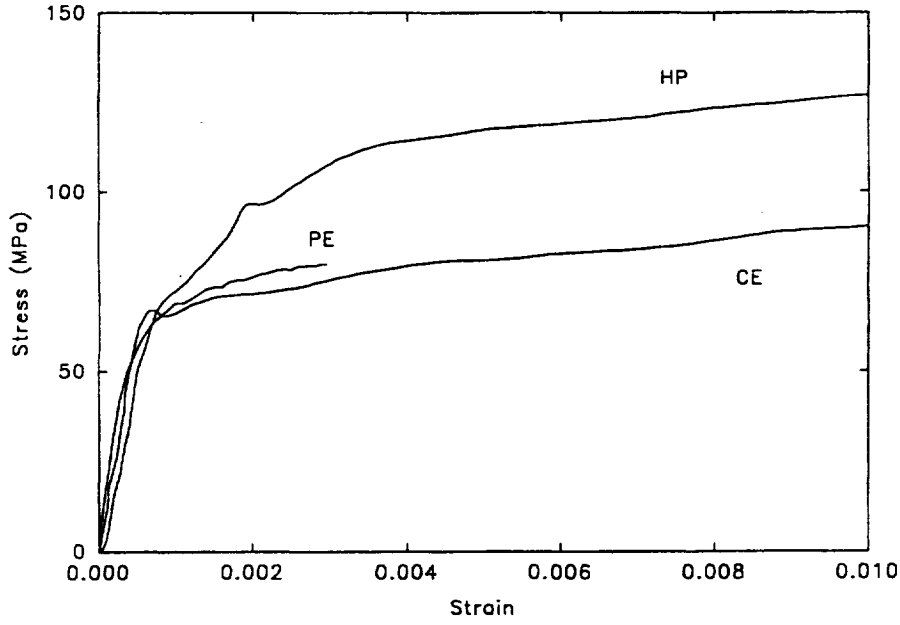

Figure 3 - Initial portion of monotonic tensile curves at 1000 K for NiAl processed by different routes.

Table II - Tensile Properties for NiAl for a Strain Rate of 1.4×10^{-3} s^{-1}

Fabrication Method	Temperature, (K)	Elastic Modulus, (GPa)	0.2% Yield Stress, (MPa)	Ultimate Tensile Strength, (MPa)	Failure Strain, (%)	BDTT, K [Refs.]
HP	300	240	-	256	0	900 [24]
	1000	160	75	-	>25	
PE	1000	126	80	-	>25	620-670 [7,14]
OE	300	230	216	270	0.85	620 [14]
	1000	140	67	-	>25	

and 140 GPa for the HP, PE and CE NiAl, respectively. The HP material yields at a 40% greater stress compared to the PE and CE materials (Table II). Additionally, each material exhibits a slight yield point (Fig. 3). Although the UTS was not captured at 1000 K (since only the initial portion of the stress-strain curve was recorded), the material did not harden substantially, and therefore the UTS is not expected to be much larger than the 0.2% yield strength.

Stress response during cyclic loading

Typical hysteresis loops for CE NiAl at 300 K are shown in Fig. 4a for a sample tested at a total strain range of 0.44%. During the first cycle a yield point and some discontinuous

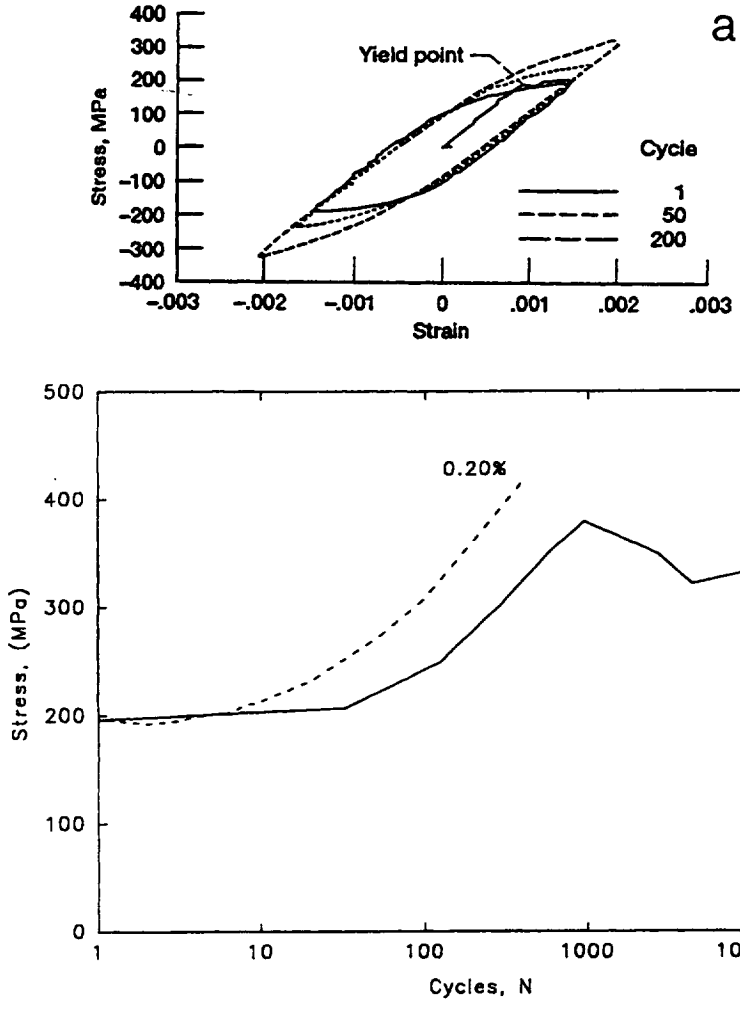

Figure 4 - a) Hysteresis loops for CE material tested at 300 K ($\Delta\epsilon_t$= 0.44%); b) response stress for CE material tested at 300 K for two strain ranges.

yielding was observed. This yield point was also present in the compressive portion of the loop in subsequent cycles, although to a lesser extent, until after about a hundred cycles the curves became very smooth. The cyclic stress responses at two strain levels, obtained by plotting the tensile peak stress from the hysteresis loops against the respective number of cycles, are shown in Fig. 4b. At 300K, the CE alloy exhibited rapid cyclic hardening to a maximum stress, followed by, at low strain ranges, a decrease in stress and then a secondary hardening peak preceding fracture.

Fig. 5 illustrates the effect of processing and applied strain range on the cyclic stress response of NiAl at 1000 K. Under identical loading conditions, the HP alloy generally displayed higher response stresses compared to PE and CE materials. The HP alloy exhibited a short period of cyclic hardening followed by a long period of gradual softening at high strain ranges, the stress maximum was attained within 10 cycles. At low strain ranges the hardening period was extended. The stress response curves of both PE and CE material resemble the behavior shown by the HP alloy at high strain ranges. Irrespective

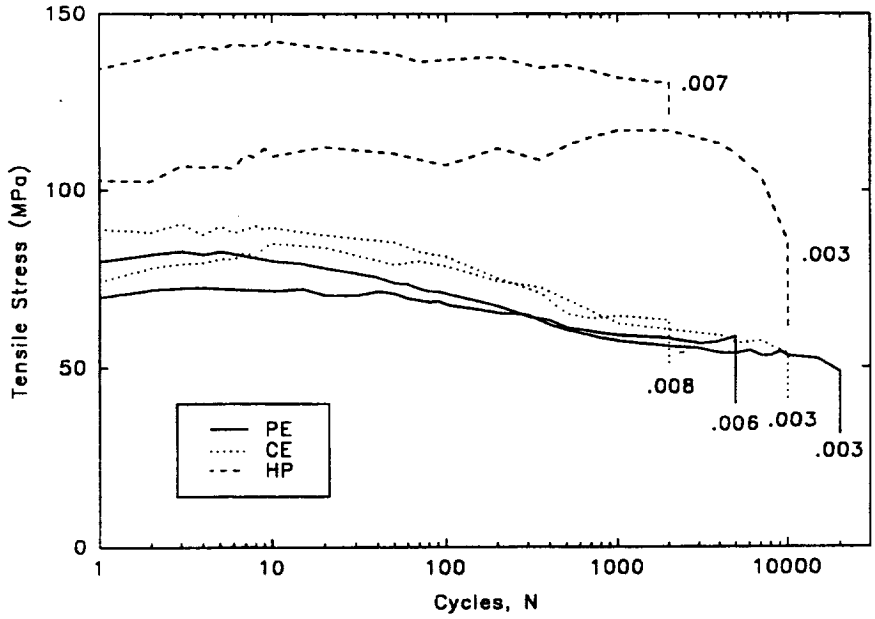

Figure 5 - Effect of processing on stress response of NiAl at 1000 K.

of the material and testing conditions, however, the amount of hardening or softening observed at 1000 K was very small, with the largest change in stress being only 35 MPa (excluding the rapid drop-off at failure). This is considerably less than the 200-300 MPa increase in stress that was observed during room temperature fatigue testing of CE NiAl (Fig. 4b).

Cyclic stress-strain behavior

Cyclic stress-strain curves (CSSC) at 1000 K for all three NiAl conditions are given in Fig. 6. It is observed that the cyclic stress-strain relationship can be represented by a power law of the form:

$$\Delta\sigma/2 = K' (\Delta\epsilon_p/2)^{n'}$$

where $\Delta\sigma/2$ = tensile stress amplitude at half-life
K' = cyclic strength coefficient
n' = cyclic strain hardening exponent
$\Delta\epsilon_p/2$ = plastic strain amplitude at half-life

The values of K' and n' are included in Table III for all three processing routes. The HP NiAl was much stronger as exemplified by a higher K' value; its n' value is also higher. The extruded versions of NiAl have identical strength and strain hardening characteristics. The CSSC of CE NiAl at 300 K (Table III), shows a low value of n' compared to the values obtained at 1000 K. Also, the K' value is significantly higher at 300 K due to the higher yield strength and the material's high work hardening rate.

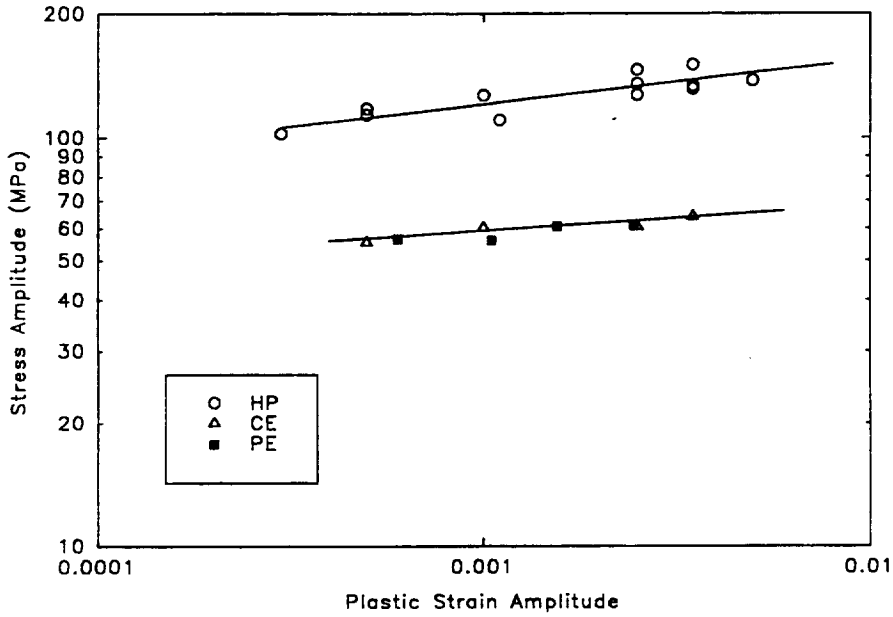

Figure 6 - Cyclic stress - strain curves for different processing conditions at 1000 K.

Table III - Constants and Exponents in Cyclic Stress-Strain and Coffin-Manson Relationships

Temp., (K)	Processing Condition	Cyclic stress-strain n'	K' (MPa)	Coffin-Manson ϵ'_f	c
300	CE	0.03	468	.006	-0.22
1000	CE	0.06	90	13.0	-0.89
1000	PE	0.06	90	0.9	-0.63
1000	HP	0.11	254	1.6	-0.73

Low cycle fatigue life

The fatigue life curves for the three NiAl materials tested at 1000 K are depicted in Figures 7-9. The life data obtained on CE material at 300 K is also included in Figs. 7-9 to

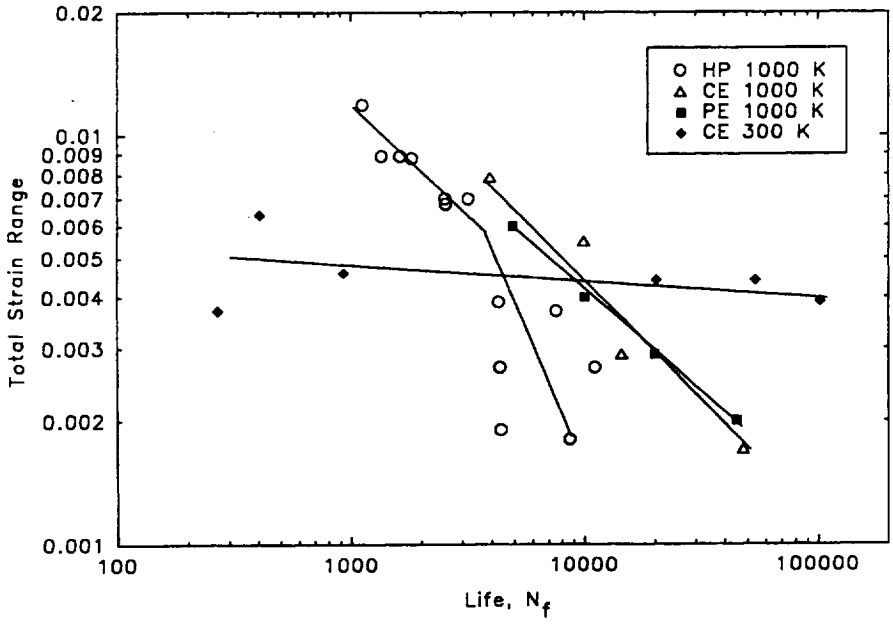

Figure 7 - Fatigue life curves on a total strain range basis.

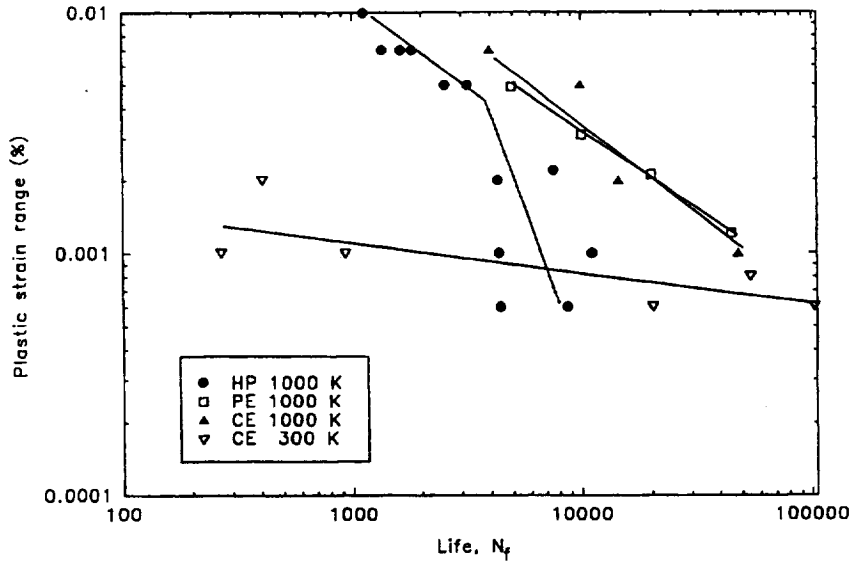

Figure 8 - Fatigue life curves on a plastic strain range basis.

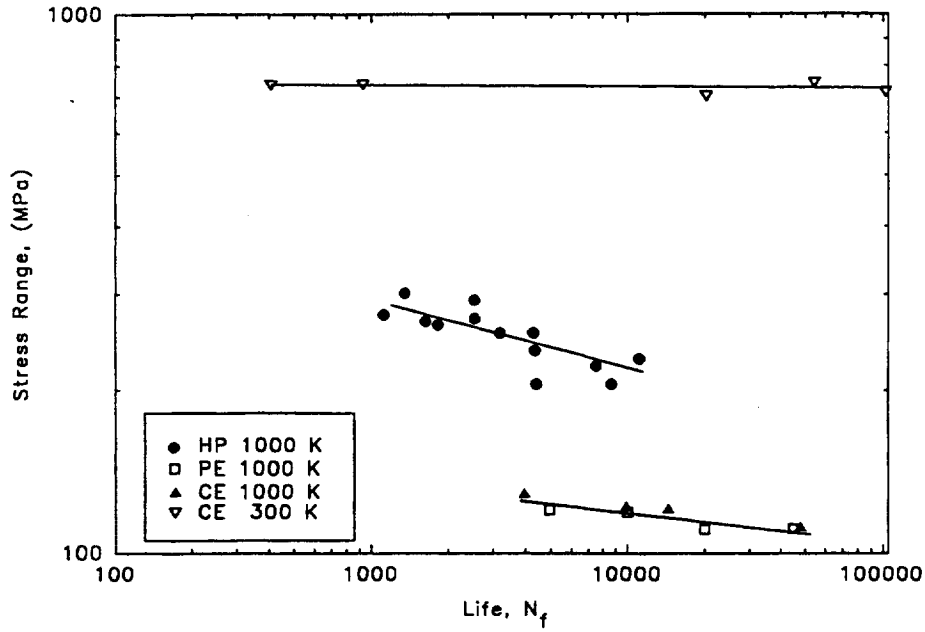

Figure 9 - Fatigue life curves on a stress range basis.

facilitate a comparison. On a total strain range basis (Fig. 7), the difference in failure life between PE and CE alloys is very small at 1000 K. The LCF lives of the HP alloy were much shorter than the extruded alloys, with a considerable reduction in life at lower strain ranges. The plastic strain fatigue resistance of the extruded materials was found to obey the Coffin-Manson relationship, $(\Delta\epsilon_p)\ N_f^c = \epsilon_f'$, where ϵ_f' and c are the fatigue ductility coefficient and fatigue ductility exponent, respectively. However, the Coffin-Manson plot (Fig. 8) of the HP NiAl shows a two slope behavior, and at plastic strain ranges ≤ 0.004, the LCF life was much lower than what could have been obtained by extrapolation from high strain regimes. Table III provides the values of the constants in the Coffin-Manson relationship for the three processing routes. The CE NiAl has a longer fatigue life at 1000 K compared to the values obtained at 300 K, especially at large strain ranges. However, this trend was reversed on a stress range basis, as depicted in Fig. 9. Data for the HP and PE conditions are also shown in Fig. 9. It should be noted that the sharp drop-off in fatigue life seen in Figs 7 & 8 for the HP material is not observed on a stress range basis.

Crack initiation, propagation and damage modes

In the HP alloy, the crack initiation and initial propagation remained intergranular at all the strain ranges. In the later stages of life, due to tensile overload, fast fracture occurred by transgranular cleavage. Roughly, 20-40% of the fracture surface of the HP alloy was due to slow intergranular fatigue crack growth, which could be easily identified by a dark ring on the sample surface as a result of oxidation (Fig. 10a). At low strain ranges, a high percentage of grain boundaries were decorated with pear shaped voids (Fig. 10b), which

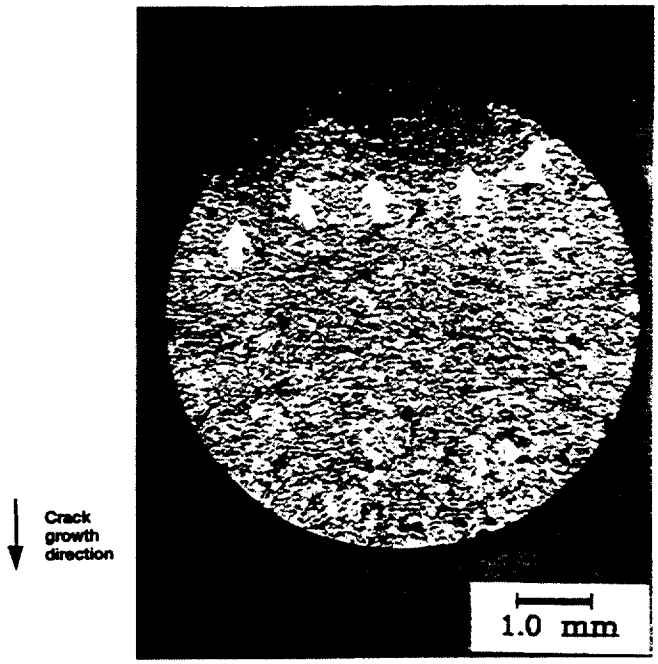

Figure 10 - a) Fracture surface of HP sample tested at 1000 K. Arrows indicate extent of slow crack growth.

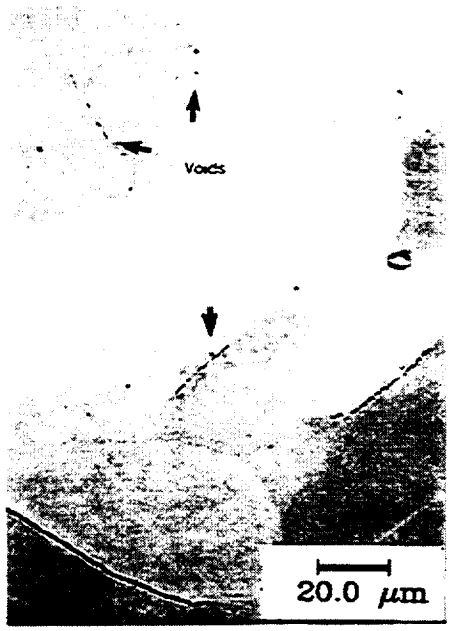

Figure 10 - b) Grain boundary voids in HP specimen tested at 1000 K.

could be regarded as damage due to creep. However, the grain boundaries that cavitated did not show any particular angular relationship with respect to the applied stress axis. At higher strain ranges, the gage surface portions of deformed samples revealed a significant number of intergranular secondary cracks and slip bands in the intragranular regions (Fig.11). At low strain ranges, the density of secondary cracks was much lower with no evidence of gross slip bands in the grain interiors.

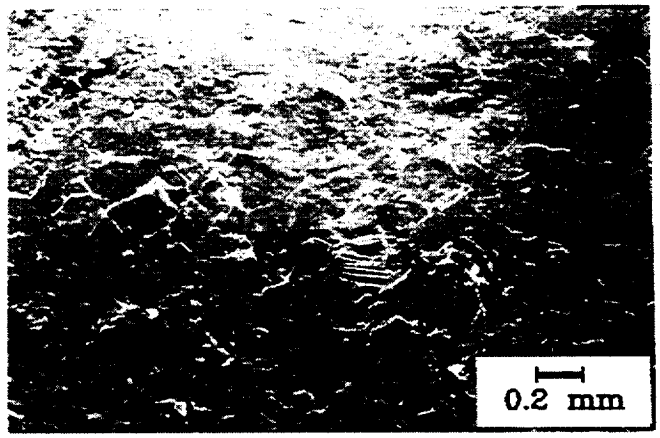

Figure 11 - SEM micrograph of HP specimen tested at 1000 K ($\Delta\epsilon_t$= 0.88%) showing the presence of secondary cracks and intragranular slip on the gage surface.

The PE NiAl exhibited intergranular fracture at all strain ranges. Characterization of the surface of fatigue tested samples showed brittle decohesion of the grain boundaries primarily in a direction perpendicular to the stress axis (Fig. 12a). The number of grain boundary

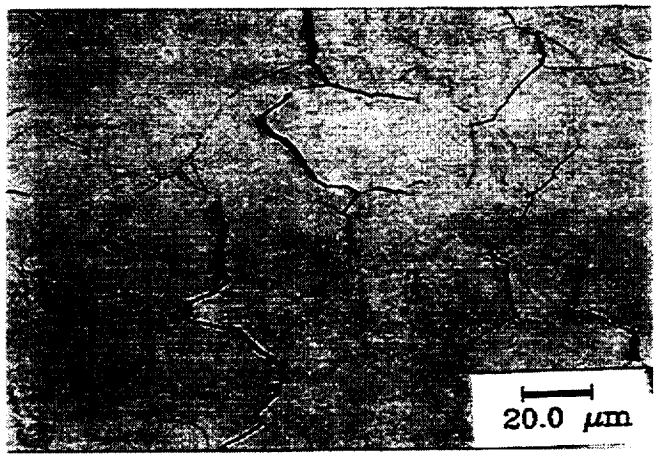

Figure 12 - a) SEM micrograph showing brittle intergranular decohesion on the gage surface of a PE specimen tested at 1000K.

cracks was extremely high and propagation occurred by interlinkage of these intergranular cracks. The operation of this process has led to the coarse step like appearance of the fracture surface as illustrated in Fig. 12b.

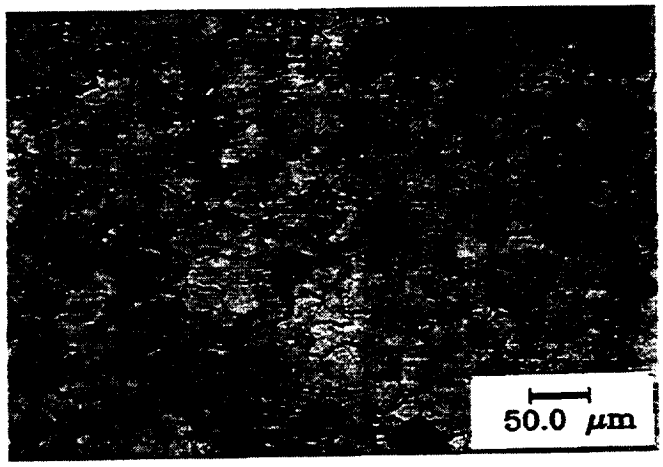

Figure 12 - b) Back scattered SEM micrograph depicting intergranular fracture in a PE specimen tested at 300 K ($\Delta\epsilon$= 0.44%).

Stable intergranular crack growth persisted over approximately 80% or more of the fracture surface of the CE material at 1000 K, regardless of the applied total strain range. The longitudinal sections of failed specimens revealed a high density of pores similar to those observed in the HP specimens. These pores were found throughout the gage section and provided a means of easy crack propagation from grain to grain. During LCF testing, the microstructure of the CE alloy was unstable and led to massive grain growth [24]. Results from experiments in which testing was interrupted after 785 cycles (10% of N_f) indicated that failure initiated by the simultaneous formation of several intergranular cracks on the surface. These observations suggest that the majority of life is spent in crack growth. It should be noted, that grain growth did not occur in the HP and PE samples.

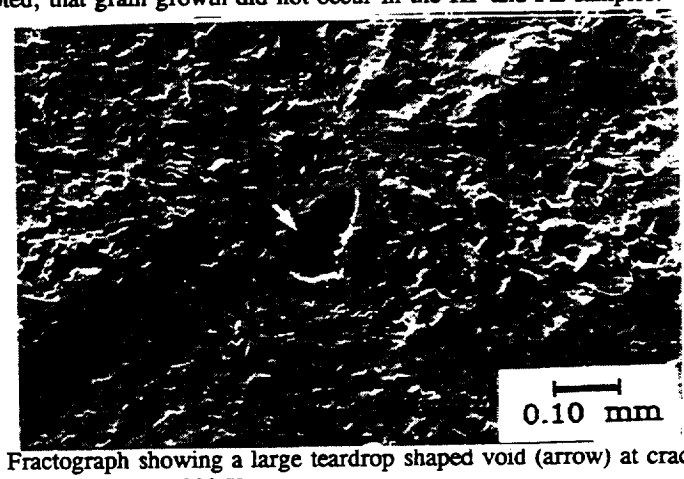

Figure 13 - Fractograph showing a large teardrop shaped void (arrow) at crack initiation site in CE specimen tested at 300 K.

At 300 K, the CE material experienced transgranular crack initiation and mixed-mode crack propagation. In all cases where fractography was performed, the fracture initiated from casting defects such as voids (Fig. 13). The CE NiAl at 300 K revealed only a small number of secondary intergranular cracks, indicative of its brittle behavior.

Substructure induced by cyclic deformation

Figures 14 and 15 show the typical substructure developed in the CE material at 300 K. The substructure at low strain ranges consisted of elongated cells (Fig. 14) with randomly distributed dislocations and dislocation tangles within the cell interiors. The propensity for cell formation decreased as the strain range was increased, and the substructure was increasingly composed of dislocation patches and clustering of dislocations in the form of thick bundles and veins (Fig. 15). The dislocation veins sometimes encompassed an entire grain. The vein structure was similar to that reported by Cullers et. al. [22,23] during LCF of the CE alloy at 600 K. At 1000 K and at low strain ranges, the CE alloy developed a continuous network of cells, whose walls were composed of dislocation tangles (Fig. 16), while at the high strain ranges the cell structure was not fully developed. The PE alloy showed cell formation at all the strain ranges with a tendency to form elongated cells at low strain ranges (Fig. 17). Fine dislocation loops and dipoles could be observed at several places in the regions of low dislocation density. The deformation behavior of the HP alloy was characterized by inhomogeneously distributed areas of high and low dislocation densities. The grain interiors had a very high density of dislocation loops and dipoles (Fig. 18). The areas adjoining the grain boundaries developed a nearly complete cell network, anchored by the nearby grain boundary.

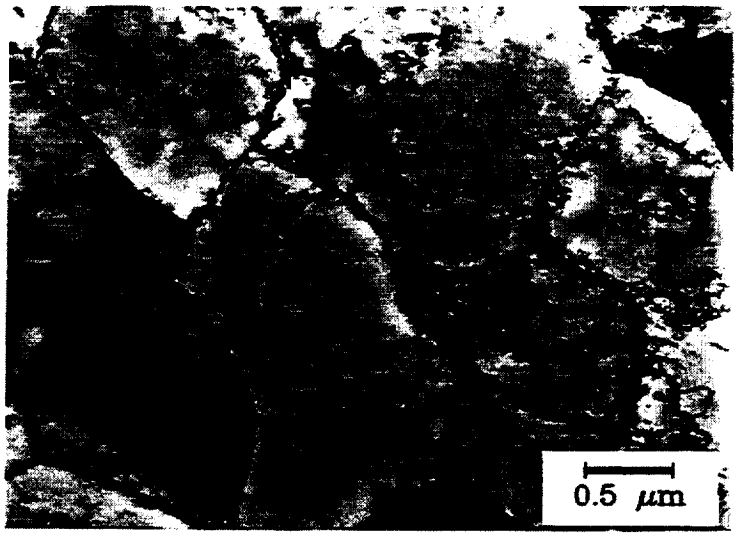

Figure 14 - Dislocation substructure consisting of cells in CE material tested at 300 K ($\Delta\epsilon_t$= 0.44%).

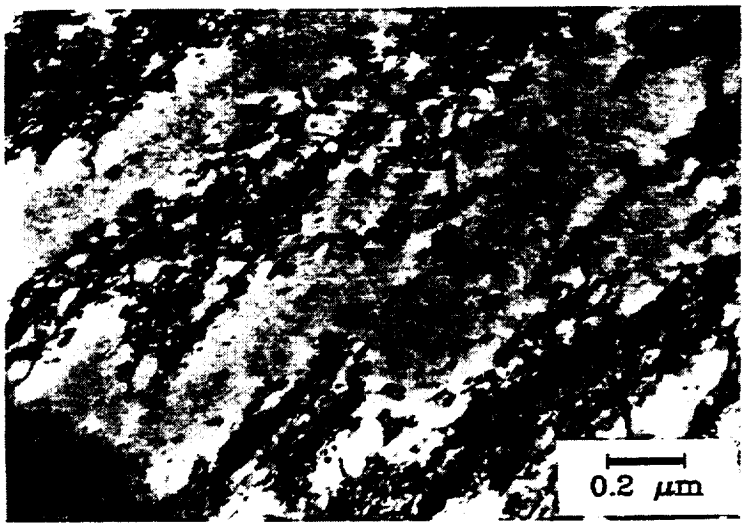

Figure 15 - Dislocation substructure in CE material tested at 300 K ($\Delta\epsilon_t$= 0.64%).

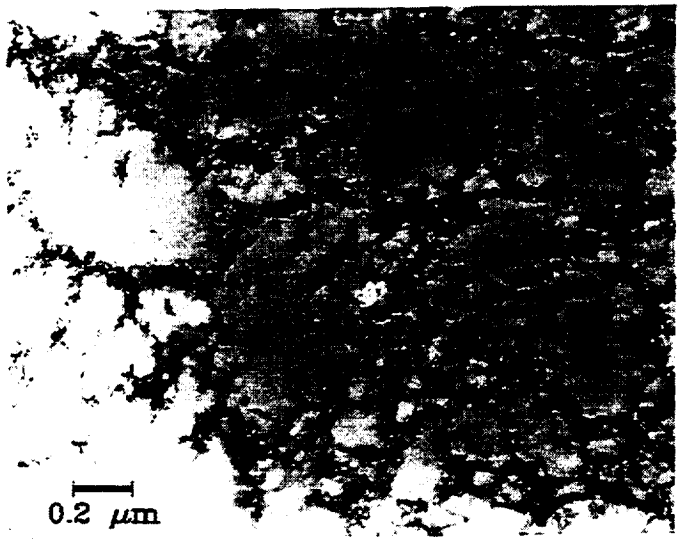

Figure 16 - Dislocation substructure composed of cells in CE material tested at 1000 K.

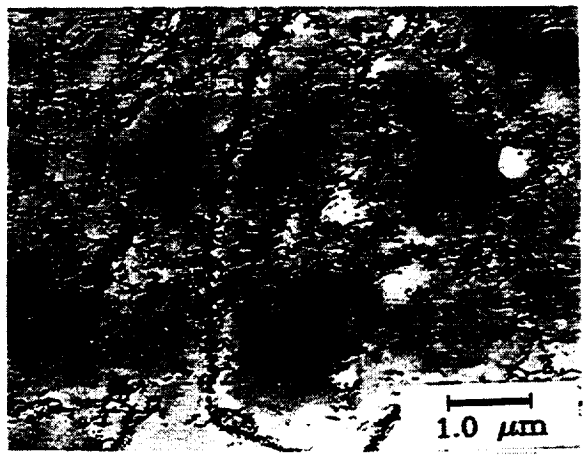

Figure 17 - Dislocation substructure in PE material tested at 1000 K ($\Delta\epsilon_t$= 0.6%).

Figure 18 - Dislocation substructure in HP material tested at 1000 K ($\Delta\epsilon_t$= 0.3%).

Discussion

Cyclic stress response and cyclic stress-strain behavior

The results clearly indicate that cyclic deformation and stress response of polycrystalline NiAl are highly sensitive to the processing route, strain range, and temperature employed during LCF testing. The fact that the cyclic stress at 1000 K remained high in the HP condition over the entire fatigue life compared to the extruded alloys, can be interpreted in terms of the operative deformation mechanisms and resulting substructural differences that were observed. In the HP alloy, the deformation substructure was composed primarily of dislocation tangles, loops and dipoles, while in contrast the substructure in the CE and PE material consisted of dislocation cells. The HP alloy showed a lesser tendency to form dislocation cells or subgrains suggesting that dislocation cross slip and climb were inhibited. Since the HP alloy had a significantly higher DBTT than the other two alloys, recovery processes are expected to be less, leading to a higher dislocation density and a more homogeneous dislocation structure in the HP material. The cyclic hardening and high response stresses and relatively higher strain hardening exponent in the HP material seems to result primarily from these differences in deformation behavior. Similarly, the cyclic softening and low strain hardening values of the two extruded materials is a direct result of the recovery process that led to the cellular dislocation substructure. In the HP alloy, the high cyclic stresses could arise from the hardening associated with the slightly higher deviation from stoichiometery observed for Heat P1418 material. The presence of Ni-antisite atoms, that result as a consequence of the slight Ni-rich deviation in stoichiometery has been reported to increase the hardness and flow stress of NiAl [2-4], as well as its BDTT [12,14].

The cyclic stress response of the CE alloy at 300 K is considerably different than what has been observed at 1000 K and is characterized by pronounced hardening. Regions of rapid hardening were also observed by Cullers et. al. [22,23] in tests performed near the BDTT. By conducting interrupted tests, these authors were able to show that the substructure changes from cells in the stress saturation domain, to well aligned dislocation veins in the rapid hardening domain that immediately preceded failure. The substructure at 300 K in the current investigation also contained dislocation veins.

Fatigue life and failure behavior

The combination of mechanical test data, stress response curves, and fractographic information enabled conclusions to be drawn about the various factors that control the cyclic life of NiAl at 1000 K. The fatigue life curves in Figs. 7 & 8 indicate that the HP alloy has shorter lives, by approximately a factor of 3, compared to the extruded alloys. All three materials displayed intergranular crack initiation and propagation, but the extent that intergranular cracking propagated before the onset of cleavage overload fracture varied substantially. The high response stresses in the HP alloy can lead to a large stress concentration at the crack tip, which would account for increased crack growth rates and hence a reduced number of cycles in the crack propagation stage. Higher response stresses would also act to reduce the critical crack size for final fracture reducing the number of cycles to failure. The HP alloy, in fact, had a much smaller zone of slow and stable intergranular crack growth compared to the extruded alloys. This observation suggests that unstable crack propagation has set in much earlier in the HP alloy.

At high plastic strain ranges, the slope of the Coffin-Manson plots (Fig. 8) were approximately equal, indicating that the mechanisms responsible for limiting life were similar in all the conditions. At plastic strain ranges below 0.3%, a change in the slope of the HP alloy became apparent. Non-ideal strain-life behavior resulting in a discontinuity has also been observed in several nickel-base superalloys [36-38], aluminum alloys [39], magnesium alloys [40], and dual-phase steels [41]. The bilinear nature of the plots has been correlated with: (i) the differences in crack initiation and propagation modes at low and high strain ranges, (ii) the differences in deformation mechanisms and (iii) the synergistic interaction between fatigue, creep and oxidation.

In the current study, in the long life regime (low strain ranges), there was significant interaction between fatigue and other time dependent processes (i.e., oxidation and creep) compared with that at low lives (high strain ranges). Analysis of longitudinal sections clearly revealed the occurrence of intergranular creep cavities, but no triple point wedge cracks, in all the processed conditions. Though quantitative assessments have not been made, it is to be expected that the HP alloy will contain a larger number of these cavities due to the presence of the alumina particles on the boundaries. It is well established that secondary phases on the grain boundary provide suitable nucleation sites for intergranular cavities [27-29,42]. These isolated creep cavities grow by the diffusional transport of vacancies or by the deformation of matrix material and, therefore, do not necessarily require grain boundary sliding. In fact, the stress concentrations in the grain boundary regions will not be easily relieved in the HP alloy due to the limited amount of recovery and this could become a contributory factor for stress assisted diffusional growth of voids.

An air environment also plays an active role in accelerating damage during fatigue at 1000 K and is, therefore, another factor contributing to a reduction in fatigue life [24]. The true effect of environment can be assessed from comparative evaluation of tests conducted in air and vacuum: if the endurance is increased in vacuum, then it may be generally construed that environment was responsible for the initial life degradation. A factor of almost three increase in life was observed for the HP material when run in vacuum (1×10^{-6} torr) compared to testing in air [24]. However, the two slope behavior still persisted in vacuum and the samples at low strain ranges also succumbed to intergranular creep cavitation. These observations suggest that the sharp decline in the life of the HP alloy at low strain ranges in air is a result of a strong synergy between fatigue, creep and oxidation.

Environmental damage during fully reversed loading at high temperatures has been shown by several investigators to play a significant role in governing fatigue life [27-29,45-48]. The acceleration of intergranular initiation and propagation in oxidizing environments is related to the existence of the grain boundary as a path for fast diffusion and chemical reactions [28,43]. The absorption and inward diffusion of the oxygen atoms down the grain boundaries can cause a reduction in surface energy and, presumably, in the cohesive strength across the grain boundary [44]. This effect may initiate sliding in the contaminated boundary and hence promote subsequent cracking. Such effects were observed in all three NiAl materials.

So far, the role of oxide particles has not been seriously considered. There is ample evidence to suggest that the LCF life is related to the size, shape and location of microstructural defects in stainless steels [49] and superalloys [50,51]. One recent study has indicated that porosity and inclusions will reduce strain controlled fatigue life of austenitic stainless steel welds by a factor of seven relative to sound weld metal [49]. The

probabilistic distribution and location of such defects also increases the scatter of LCF life. The oxide particles in the HP alloy are a source of concern and could initiate cracks under cyclic loading in the first cycle. Therefore, the variation of the oxide particles in the HP samples could be expected to be a large source of scatter in the LCF life of HP specimens tested at low strain ranges leading to the apparent discontinuity in strain-life behavior. Therefore, a very large number of specimens would have to be tested to get reliable life results for the HP alloy at low strain ranges. In order to improve the fatigue life of the HP alloy, strict control over the powder cleanliness needs to be exercised.

Conclusions

Based on the detailed investigations conducted on the low cycle fatigue behavior of polycrystalline NiAl at 1000 K, the following conclusions can be drawn:

a) Typically all three NiAl materials exhibited relatively little cyclic hardening or softening at 1000 K. However, the HP alloy displayed a higher cyclic stress response at all the strain ranges.

b) The higher stress response in the HP alloy has been attributed to a more homogeneous dislocation substructure, to the presence of significant dislocation debris, and a possible deviation in stoichiometery. The lower stress response of the extruded alloys seems to result from the occurrence of cross slip, dislocation climb, and the consequent arrangement of dislocations into cells. These differences in substructure were traced to the proximity of the fatigue test temperature to each material's DBTT.

c) Cast plus extruded and powder extruded alloys exhibited similar lives under identical strain ranges. The HP alloy had much lower lives than the extruded materials, with an increasing difference in life at lower strain ranges.

d) Plastic strain fatigue resistance for all the materials, regardless of processing route, could be described by a Coffin-Manson relationship. The HP alloy exhibited a break in the Coffin-Manson curve, in which the fatigue lives at low strain ranges were much shorter than those expected by extrapolation from high strain range portions of the curve.

e) The large reduction in life at low strain ranges in the HP alloy is suggested to result from the synergistic interactions between fatigue, creep and oxidation damage in addition to the presence of prior particle boundaries and a higher response stress.

f) Crack initiation and propagation in all the processing conditions occurred intergranularly and was aided by environmental degradation.

Acknowledgements

The authors wish to thank Dr. G. R. Halford for many helpful discussions and encouragement. K. Bhanu Sankara Rao wishes to acknowledge the National Research Council, Washington, D.C. for granting the fellowship. The diligent efforts of Mr. Ralph Corner in the fatigue laboratory are greatfully acknowledged.

References

1. R. Darolia, "NiAl Alloys for High-Temperature Structural Applications," J. Metals, 43 (3), 1991, 44-49.

2. D.B. Miracle, "The Physical and Mechanical Properties of NiAl," Acta Metall. Mater., 41, 1993, 649-684.

3. R.D. Noebe, R.R. Bowman and M.V . Nathal, "Review of the Physical and Mechanical Properties of the B2 Compound NiAl," Int. Mater. Rev., 38, 1993, 193-232.

4. R.D. Noebe, R.R. Bowman and M.V. Nathal, "Physical and Mechanical Metallurgy of NiAl," NASA TP-3398, 1994.

5. A. Ball and R.E. Smallman, "The Operative Slip System and General Plasticity of NiAl," Acta Metall., 14, 1966, 1517-1526.

6. R.R. Bowman, R.D. Noebe, S.V. Raj and I.E. Locci, "Correlation of Deformation Mechanisms with the Tensile and Compressive Behavior of NiAl and NiAl(Zr) Intermetallic Alloys," Metall. Trans. A, 23A, 1992, 1493-1508.

7. R.D. Noebe, "The Effect of Various Metallurgical Parameters on the Flow and Fracture Behavior of Polycrystalline NiAl Near the Brittle-To-Ductile Transition," NASA TM-106534, 1994.

8. R. Darolia, D.F. Lahrman and R.D. Field, "The Effect of Iron, Gallium and Molybdenum on the Room Temperature Tensile Ductility of NiAl," Scripta Metall. Mater., 26, 1992, 1007-1012.

9. K. Matsugi, D.W. Wenman and N.S. Stoloff, "Observation of the Brittle to Ductile Transition Temperature in the Iron Microalloyed Polycrystalline NiAl Intermetallic Compound," Scripta Metall. Mater., 27, 1992, 1633-1638.

10. R.D. Noebe and M.K. Behbehani, "The Effect of Microalloying Additions on the Tensile Properties of Polycrystalline NiAl," Scripta Metall. Mater., 27, 1992, 1795-1800.

11. J.D. Cotton, R.D. Noebe and M.J. Kaufman, "Chromium Bearing NiAl Intermetallic Alloys," Intermetallics, 1, 1993, 3-20 and 117-126.

12. K.H. Hahn and K. Vedula, "Room Temperature Tensile Ductility in Polycrystalline B2 NiAl," Scripta Metall., 23, 1989, 7-12.

13. E.P. George and C.T. Liu, "Brittle Fracture and Grain Boundary Chemistry of Microalloyed NiAl," J. Mater. Res., 5, 1990, 754-762.

14. R.D. Noebe, C.L. Cullers and R.R. Bowman, "The Effect of Strain Rate and Temperature on the Tensile Properties of NiAl," J. Mater. Res., 7, 1992, 605-612.

15. P. Nagpal and I. Baker, "The Effect of Grain Size on the Room Temperature Ductility of NiAl," Scripta Metall. Mater., 24, 1990, 2381-2384.

16. S. Reuss and H. Vehoff, "Temperature Dependence of the Fracture Toughness of Single Phase and Two Phase Intermetallics," Scripta Metall. Mater., 24, 1990, 1021-1026.

17. H. Vehoff, "Fracture Mechanisms in Intermetallics," in Ordered Intermetallics - Physical Metallurgy and Mechanical Behavior, ed. C.T. Liu et al., NATO ASI Series E, Vol. 213, Kluwer Academic Publishers, 1992, 299-320.

18. R.D. Noebe, M. Hebsur, J.D. Whittenberger, M.V. Nathal and B. Oliver, "Fracture Toughness Limits In Polycrystalline NiAl-Based Materials and Potential Directions for Developing Improved Alloy Systems" to be published in HITEMP Review 1994, NASA CP, 1994.

19. J.D. Cotton and R.W. Margevicius, "Study of the Brittle-to-Ductile Transition in NiAl by Texture Analysis," accepted Acta Metall. Mater., 1994.

20. R.D. Noebe and B.A. Lerch, "Room Temperature Cyclic Deformation Behavior of Cast and Extruded NiAl," Scripta Metall. Mater., 27, 1992, 1161-1166.

21. K.M. Edwards and R. Gibala, "Low-Cycle Fatigue Behavior of Polycrystalline NiAl at Room Temperature," in High Temperature Ordered Intermetallic Alloys V, ed. I. Baker et al., Mater. Res. Soc. Symp. Proc. Vol. 288, 1993, 665-670.

22. C.L. Cullers, S.D. Antolovich and R.D. Noebe, "Deformation Behavior of Polycrystalline NiAl Cyclically Deformed Near the Brittle-to-Ductile Transition Temperature," in High Temperature Ordered Intermetallic Alloys V, ed. I. Baker et al., Mater. Res. Soc. Symp. Proc. Vol. 288, 1993, 531-536.

23. C.L. Cullers, "Deformation Mechanisms of NiAl Cyclicly Deformed Near the Brittle-to-Ductile Transition Temperature", NASA CR-191121, 1993.

24. B.A. Lerch and R.D. Noebe, "Low Cycle Fatigue Behavior of Polycrystalline NiAl at 1000 K," Metall. Mater. Trans. A, 25A, 1994, 309-319. (Also NASA TM-105987, 1993).

25. J.C. Lautridou, J.Y. Guedou and Y. Honnorat, "Effect of Inclusions on LCF Life of PM Superalloys for Turboengine Discs," High Temperature Materials for Power Engineering 1990, Kluwer Academic Publishers, London, 1990, 1163-1172.

26. K. Bhanu Sankara Rao, M. Valsan, R. Sandhya, S.L. Mannan and P. Rodriguez, "Study on the Significance of Weld Discontinuities in Low Cycle Fatigue of Austenitic Stainless Steel", Proc. Intl. Conf. on Fatigue and Fracture in Steel and concrete Structures", Madras, 19-21, Dec.1991. Vol.2, (1991), 1501-1512.

27. K. Bhanu Sankara Rao, "Influence of Metallurgical Variables on Low Cycle Fatigue Behavior of Type 304 Stainless Steel," Ph.D. Thesis, University of Madras, India, Jan. 1989.

28. K. Bhanu Sankara Rao, M. Valsan, R. Sandhya, S.L. Mannan and P. Rodriguez, "Synergistic Interactions During High Temperature Fatigue of Type 304 Stainless Steel - Grain Size Dependence," Trans. Indian Inst. Met, 44, 1991, 255-270.

29. P. Rodriguez and K. Bhanu Sankara Rao, "Nucleation and Growth of Cracks and Cavities under Creep-Fatigue Interaction," Progress in Materials Science, 37, 1993, 403-480.

30. K. Bhanu Sankara Rao, "Time Dependent Low Cycle Fatigue Behavior of High Temperature Alloys", Trans. Indian Inst. Met, 42, 1989, s61-s82.

31. J.D. Whittenberger, "Effect of Grain Size on the High Temperature Properties of B2 Aluminides", NASA TM 101382, May 1987.

32. K. Bhanu Sankara Rao, M. Valsan, R. Sandhya, S.L. Mannan and P. Rodriguez, "Dynamic Strain Ageing Effects in Low Cycle Fatigue", High temperature Materials and Processes., 7, 1986, 171-178.

33. M. Valsan, D.H. Sastry, K. Bhanu Sankara Rao and S.L. Mannan., "Effect of Strain Rate on the High Temperature Low Cycle Fatigue Properties of a Nimonic PE-16 Superalloy", Metall. and Mat. Trans. A, 25A, 1994, 159-171.

34. H.J. Christ and H. Mughrabi, "Microstructure and Fatigue", in Low Cycle Fatigue and Elasto-Plastic Behavior of Materials-3, Eds. K.-T. Rie et al., Elsevier Applied Science, 1992, 56-69.

35. A.K. Ghosh and R. Raj, "A model for the Evolution of Grain Size Distribution During Superplastic Deformation", Acta Metall, 34, 1986, 447-456.

36. B.A. Lerch and V.Gerold, "Room Temperature Deformation Mechanisms in Nimonic 80A" Acta Metall., 33, 1985, 1709-1716.

37. M. Clavel, C. Levailant and A. Pineau., Proc. Conf. On Creep-Fatigue-Environment Interaction, Eds. R.M. Pelloux and N.S. Stoloff, The Metallurgical Society of AIME, Warrendale, Pa., 1980, 24-45.

38. M.Valsan, K. Bhanu Sankara Rao and S.L. Mannan, "Effects of Microstructure on Elevated Temperature LCF Behavior of Nimonic PE-16 Superalloy", Trans. Ind. Inst. Metals, 42 (Supplement), 1989, s203-s216.

39. T.H. Sanders and E.A. Starke. Jr., Metall Trans A, 7, 1976, 1107-1116.

40. J. Wareing, B. Tomkins and G. Sumner, in Fatigue at Elevated Temperatures, A.E. Carden, A.J. McEvily and C.H. Wells, eds., ASTM, STP, Vol.520, 1973, 123-137.

41. S.R. Mediratta, V. Ramaswamy and P. Rama Rao, "Two-Stage Cyclic Work Hardening and Two Slope Coffin-Manson Relationship in Dual Phase Steels", Scripta Metall., 20, 1986, 555-560.

42. R. Raj, "Nucleation and Growth of Cavities at Second Phase Particles in Grain Boundaries", Acta Metallurgica, 26, 1978, 995-1005.

43. J. Bressers, "Fatigue and Microstructure", in Proc. Intl. Conf. on High Temperature Alloys and Their Exploitable Potential, Oct.15-17, 1985, Joint Research Center, Petten, Netherlands.

44. J. Bressers, M. Roth, P. Tambuyser and E. Fenske, "The Effect of Time Dependent Processes on the LCF life of Gas Turbine Disc Alloys", Commission of the European Communities, Report EUR 8162 EN, 1982.

45. S. Kalluri, S.S. Manson and G.R. Halford, "Environmental Degradation of 316 Stainless Steel in High Temperature Low Cycle Fatigue", Third International Conf. on Environmental Degradation of Engineering Materials, R.P. McNitt and M.R. Louthan Jr., Eds., The Pennsylvania State University, University Park, Pa, 1987, 503-519.

46. T. Ericsson, Can. Metall. Q., 18, 1979, 177-192.

47. D. Fournier and A. Pineau, "Low Cycle Fatigue Behaviour of Inconel-718 at 298 K and 823 K", Metall. Trans. A, 8, 1977, 1095-1106.

48. C.J. Mcmahan and L.F. Coffin Jr., "Mechanisms of Damage and Fracture in High Temperature Low Cycle Fatigue of a Cast Nickel-Based Superalloy", Metall Trans.A., 1, 1970, 3443-3452.

49. K. Bhanu Sankara Rao, M. Valsan, R. Sandhya, S.L. Mannan and P. Rodriguez, "Influence of Weld Discontinuities on Strain Controlled Low Cycle Fatigue Behaviour of 308 SS Welds", Trans. ASME, Journal of Engineering Materials Technology, 116, 1994, 193-199.

50. J. Hyzack and I.M. Bernstein, "The Effect of Defects on Fatigue Crack Initiation Process in Two P/M Superalloys: Part-I, Fatigue Origins", Metall. Trans. A., 13, 1982, 33-43.

51. J. Hyzack and I.M. Bernstein, "The Effect of Defects on the Fatigue Crack Initiation Process in Two P/M Superalloys: Part-II, Surface-Subsurface Transition", Metall. Trans. A., 13, 1982, 45-52.